Research Square

Preprints are preliminary reports that have not undergone peer review.
They should not be considered conclusive, used to inform clinical practice,
or referenced by the media as validated information.

Naturally Occurring Soluble Aβ Oligomers Induce State-Dependent Hippocampal Circuit Dysfunction in Nontransgenic Mice

Hanyan Li
Massachusetts General Hospital, Harvard Medical School https://orcid.org/0000-0001-8686-339X
Aline Fassini
Massachusetts General Hospital, Harvard Medical School
Sema Aygar
Massachusetts General Hospital, Harvard Medical School https://orcid.org/0000-0001-8112-0343
Zoey Vasilakos
Massachusetts General Hospital, Harvard Medical School
Steven Hou
Massachusetts General Hospital
Midori Yokomizo
Massachusetts General Hospital
Ksenia Kastanenka
Harvard Harvard Medical School / Massachusetts General Hospital https://orcid.org/0000-0002-3727-0317
Stephen Gomperts
gomperts.stephen@mgh.harvard.edu

Department of Neurology, Massachusetts General Hospital, Harvard Medical School

Article

Keywords:

Posted Date: November 10th, 2026

DOI: https://doi.org/10.21203/rs.3.rs-11234037/v1

License: This work is licensed under a Creative Commons Attribution 4.0 International License.
Read Full License

Additional Declarations: There is **NO** Competing Interest.

Naturally Occurring Soluble Aβ Oligomers Induce State-Dependent Hippocampal Circuit Dysfunction in Nontransgenic Mice

Hanyan Li [1 2], Aline Fassini [1 2], Sema Aygar [1 2], Zoey Vasilakos [1 2], Steven S. Hou [1 2], Midori Yokomizo [1 2], Ksenia V. Kastanenka [1 2], Stephen N. Gomperts [1 2 *]

[1] Massachusetts General Hospital, Boston, Massachusetts, USA

[2] Harvard Medical School, Boston, Massachusetts, USA

*Correspondence: Gomperts.stephen@mgh.harvard.edu

Abstract

Amyloid-beta (Aβ) plaques are a hallmark of Alzheimer's Disease (AD), but the modest cognitive benefit of anti-amyloid antibodies despite plaque clearance implicates plaque-independent mechanisms in disease progression. Aβ oligomers (AβOs), a toxic soluble species, disrupt synapses, but their effects on hippocampal circuit function in vivo remain unclear. We tested whether naturally occurring AβOs are sufficient to disrupt hippocampal circuit function independent of plaques in nontransgenic mice, infusing wild-type culture medium (WtCM), Tg2576-derived culture medium containing naturally occurring human AβOs (TgCM), or Aβ-immunodepleted TgCM into CA1. We recorded hippocampal calcium activity and local field potentials as mice explored a linear track and during post-learning quiet wakefulness. During exploratory behavior, TgCM impaired theta-gamma coupling versus WtCM, without affecting running, calcium activity, or place cells. During quiet wakefulness, TgCM reduced calcium activity versus WtCM, without a detectable effect on reactivation, delta oscillations, or sharp wave ripples. Aβ depletion prevented both effects. These results suggest that AβO-induced circuit disruption depends on behavioral state, implicating distinct vulnerabilities in encoding and offline processing. Because these effects occurred in nontransgenic hippocampus without amyloid plaques or chronic transgene expression, soluble AβOs are sufficient to disrupt memory-relevant circuit function and represent a therapeutic target upstream of plaque clearance.

Introduction

Although amyloid-beta42 (Aβ) plaques are a hallmark of Alzheimer's disease (AD) [1,2], their levels correlate poorly with dementia severity [3], and their clearance with anti-amyloid antibody therapeutics is associated with only modest benefit for cognitive function [4–7]. In contrast, the levels of soluble Aβ species correlate with AD progression [8], and among those, Aβ oligomers (AβOs) are the most toxic species to cells and synapses [9–18]. However, whether naturally occurring AβOs are sufficient to cause hippocampal circuit dysfunction in vivo, independent of plaques and chronic transgene expression, is unknown.

Hippocampal circuitry supports memory processing. During online exploratory behavior, the phase of hippocampal theta oscillations modulates the amplitude of hippocampal gamma oscillations [19–22], and this phase-amplitude coupling is important for memory encoding [19–22]. Place cells encode spatial information, and their sequential activation during awake behavior (which is theta phase dependent) is recapitulated during offline behaviors such as quiet wakefulness and sleep, in highly compressed replay sequences [23–25]. This place cell reactivation is implicated in memory consolidation, planning, and learning [23–25].

Establishing a causal role for AβOs in vivo has been difficult. Synthetic and recombinant AβOs are structurally artificial and are usually applied at concentrations well above those found in AD brain. Transgenic amyloidosis models avoid this problem but introduce others. Chronic expression of mutant transgenes can drive compensatory changes over time, and the transgenes themselves are not biologically neutral: APP overexpression elevates

non-Aβ APP fragments with their own signaling activity, and mutant presenilin-1 has Aβ-independent roles in synaptic transmission and calcium signaling [26–34]. Circuit phenotypes in these models cannot be attributed to AβOs alone.

To address these problems directly, we infused naturally occurring, low molecular weight human AβOs into the hippocampus of freely behaving nontransgenic mice and used depletion and repletion of infused Aβ within the same animals to test whether AβOs specifically drive circuit changes. We recorded hippocampal calcium activity and local field potentials during active exploration and quiet wakefulness to test whether AβOs disrupt neuronal activity across states, theta-gamma coupling during exploration, and place cell reactivation during quiet wakefulness.

Results

To investigate the causal effects of AβOs on hippocampal circuit function, we injected AAV1-hSyn-GCaMP6f into the hippocampal CA1 region of nontransgenic mice and implanted an integrated lens-electrodes-cannula device (C57BL/6J, male, 4.0 ± 0.1 months old at the time of recording, n=7 mice implanted, **Fig. 1a top**). We confirmed cannula placement with infusion of DiI (Molecular Probes, 50 mg/ml, 1μL over 20 min [35]) and subsequent histology, which showed labeling in CA1 s. radiatum below the s. pyramidale imaging plane (**Fig. 1a bottom**). We recorded simultaneous dynamic calcium imaging and local field potential (LFP) targeting s. pyramidale and s. radiatum as animals freely behaved and underwent intra-hippocampal infusion (**Fig. 1b**).

AβOs impaired theta-gamma coupling during exploratory behavior

We infused 0.5 μL wild type culture medium (WtCM) over 10 minutes as each mouse ran freely on the linear track. We then infused 0.5 μL transgenic culture medium containing human AβOs (TgCM) over 10 minutes within the same animal and behavioral task (**Fig. 1b**). Run behavior was comparable between WtCM infusion and TgCM infusion (number of laps run: from 17.6 ± 2.9 to 16.6 ± 3.8 laps, mean difference=-1.00, 95% CI [-3.83, 1.83], paired t(6)=-0.87, p=0.420, Cohen's d=-0.33; run velocity: from 6.0 ± 0.7 to 5.8 ± 1.0 cm/s, mean difference=-0.21, 95% CI [-0.99, 0.57], paired t(6)=-0.65, p=0.539, Cohen's d=-0.25. **Fig. 1c**). The average calcium event rate across all cells did not differ significantly between WtCM infusion and TgCM infusion (from 1.2 ± 0.2 to 1.3 ± 0.1 spikes/min, mean difference=0.05, 95% CI [-0.25, 0.35], paired t(5)=0.45, p=0.670, Cohen's d=0.18. **Fig. 1d**). We then investigated place cells and found no statistically significant difference in their proportions, calcium event rate, spatial information or field width between WtCM infusion and TgCM infusion (Place cell proportion: from 0.2 ± 0.0 to 0.2 ± 0.0, mean difference=0.02, 95% CI [-0.08, 0.11], paired t(5)=0.47, p=0.658, Cohen's d=0.19; place cell calcium event rate: from 1.6 ± 0.2 to 1.5 ± 0.1 spike/min, mean difference=-0.13, 95% CI [-0.51, 0.24], paired t(5)=-0.91, p=0.405, Cohen's d=-0.37; spatial information: from 2.3 ± 0.2 to 2.4 ± 0.2 bit/s, mean difference=0.05, 95% CI [-0.20, 0.30], paired t(5)=0.53, p=0.618, Cohen's d=0.22; place field width: from 20.6 ± 3.0 to 17.5 ± 1.0 cm, mean difference=-3.15, 95% CI [-10.55, 4.25], paired t(5)=-1.09, p=0.324, Cohen's d=-0.45. **Fig. 1e**). Theta power trended lower with TgCM infusion compared to WtCM infusion, while gamma power was comparable between conditions (theta power:

(8.4 ± 1.1) × 10^{-3} to (6.9 ± 0.8) × 10^{-3}, mean difference=-1.54 × 10^{-3}, 95% CI [-3.18, 0.10] × 10^{-3}, paired t(6)=-2.30, p=0.061, Cohen's d=-0.87; gamma power: from (6.6 ± 0.8) × 10^{-4} to (6.9 ± 0.8) × 10^{-4}, mean difference=0.29 × 10^{-4}, 95% CI [-1.16, 1.74] × 10^{-4}, paired t(6)=0.48, p=0.646, Cohen's d=0.18. **Fig. 1f**). Theta-gamma phase-amplitude coupling (PAC) was significantly reduced with TgCM infusion compared to WtCM infusion (from 1012.4 ± 247.1 to 881.4 ± 225.7 modulation index (MI), mean difference=-130.99, 95% CI [-213.79, -48.19], paired t(6)=-3.87, p=0.008, Cohen's d=-1.46. **Fig. 1g**). We noted no behavioral or electrical seizure-like events, epileptiform spikes, or sharp waves with TgCM infusion.

Because AβO effects might persist, precluding a clean reversed-order comparison with subsequent infusion of WtCM, we instead assessed nonspecific temporal drift using sequential 0.5 µL artificial cerebrospinal fluid (aCSF) infusions as animals performed the task (**Fig. 1h**). Run behavior did not differ significantly between the first and second infusions, showing only nonsignificant trends towards fewer laps and slower running (run lap number: from 9.9 ± 0.9 to 9.3 ± 1.1 laps, mean difference=-0.57, 95% CI [-1.30, 0.16], paired t(6)=-1.92, p=0.103, Cohen's d=-0.73; run velocity: from 4.6 ± 0.3 to 4.4 ± 0.4 cm/s, mean difference=-0.27, 95% CI [-0.59, 0.05], paired t(6)=-2.05, p=0.086, Cohen's d=-0.78. **Fig. 1i**), with no significant difference in theta and gamma power (theta power: from (8.6 ± 1.8) × 10^{-3} to (7.8 ± 1.9) × 10^{-3}, mean difference=-0.78 × 10^{-3}, 95% CI [-5.48, 3.93] × 10^{-3}, paired t(6)=-0.40, p=0.701, Cohen's d=-0.15; gamma power: from (5.5 ± 0.8) × 10^{-4} to (5.8 ± 0.6) × 10^{-4}, mean difference=0.28 × 10^{-4}, 95% CI [-1.00, 1.55] × 10^{-4}, paired t(6)=0.53, p=0.616, Cohen's d=0.20. **Fig. 1j**). In addition, theta-gamma coupling during

the first and second infusions of aCSF was comparable (from 1471.9 ± 184.7 to 1386.6 ± 173.6 MI, mean difference=-85.24, 95% CI [-194.67, 24.19], paired t(6)=-1.91, p=0.105, Cohen's d=-0.72. **Fig. 1k**). Thus, although modest within-session slowing may occur over paired acquisitions, it was not accompanied by drift in theta-gamma coupling, in theta or gamma power, or in the principal offline neuronal outcomes (**Fig. 3g, h**). These results show that infused AβOs impair theta-gamma coupling, a hippocampal circuit phenomenon that contributes to memory encoding.

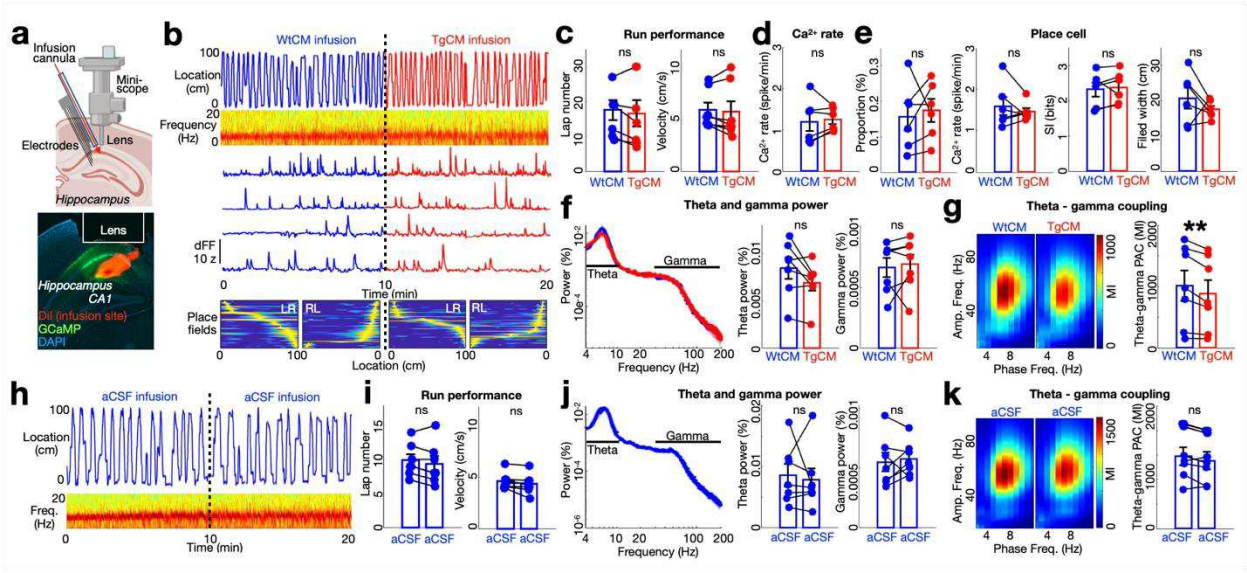


Figure 1. AβOs impaired theta-gamma coupling. a) Top: An integrated lens-electrodes-cannula device was implanted in the hippocampal CA1 region of mice injected with AAV-hsyn-GCaMP6f to enable calcium imaging, local field potential recording, and local infusions. Bottom: DiI labeling confirms the infusion site in CA1 stratum radiatum, immediately below the stratum pyramidale imaging plane. **b)** From top to bottom: Examples of run behavior on the linear track as a function of time, associated CA1 s. radiatum spectrograms, dynamic calcium traces, and sorted place fields in left-right (LR)

and right-left (RL) directions during WtCM infusion (blue), followed by TgCM infusion (red); representative data from one mouse. **c)** The number of laps run (left) and run velocity (right) were similar with WtCM and TgCM infusion. **d)** Average calcium event rates were similar with WtCM and TgCM infusion. **e)** From left to right, place cell proportion, calcium event rate, spatial information and field width were similar with WtCM and TgCM infusion. **f)** Theta and gamma band power were comparable with WtCM and TgCM infusion. **g)** Theta-gamma phase-amplitude coupling was significantly reduced with TgCM infusion compared to WtCM infusion. **h)** Examples of run behavior on the linear track as a function of time (top), associated CA1 s. radiatum spectrograms (bottom) during sequential aCSF infusions (blue); representative data from one mouse. **i)** The number of laps run (left) and running velocity (right) were similar with sequential infusions of aCSF. **j)** Theta and gamma band power were similar with sequential infusions of aCSF. **k**) Theta-gamma coupling was unchanged with sequential infusions of aCSF. ns, $p>0.05$, ** $p<0.01$, two-sided paired t-tests. n=7 mice for c, f, g, i, j, k; n=6 mice, 451 ± 202 cells and 58 ± 23 place cells for d, e. Data are shown as mean ± SEM.

Aβ depletion abolished AβO-induced theta-gamma coupling impairment

To confirm the impact of AβOs on theta-gamma coupling, we depleted Aβ from TgCM (depleted-TgCM, see Methods) and infused depleted-TgCM into the hippocampus. This depletion resulted in 96.7% Aβ removal (**Supplementary Fig. 1**).

We infused 0.5 µL WtCM over 10 minutes as the mouse ran on the linear track, and then infused 0.5 µL depleted-TgCM over 10 minutes within the same animal and behavioral

task (**Fig. 2a**). Run behavior was comparable with WtCM and depleted-TgCM infusions (run lap number: from 13.7 ± 2.0 to 13.0 ± 2.3 laps, mean difference=-0.67, 95% CI [-2.62, 1.29], paired t(5)=-0.88, p=0.421, Cohen's d=-0.36; run velocity: from 4.6 ± 0.6 to 4.4 ± 0.7 cm/s, mean difference=-0.17, 95% CI [-0.68, 0.35], paired t(5)=-0.83, p=0.445, Cohen's d=-0.34. **Fig. 2b**). The power of theta and gamma bands was comparable under WtCM infusion and depleted-TgCM infusion (theta power: from (1.1 ± 0.2) × 10^{-2} to (1.0 ± 0.2) × 10^{-2}, mean difference=-0.06 × 10^{-2}, 95% CI [-0.39, 0.27] × 10^{-2}, paired t(5)=-0.47, p=0.661, Cohen's d=-0.19; gamma power: from (7.6 ± 1.4) × 10^{-4} to (7.3 ± 1.6) × 10^{-4}, mean difference=-0.32 × 10^{-4}, 95% CI [-2.20, 1.55] × 10^{-4}, paired t(5)=-0.44, p=0.677, Cohen's d=-0.18. **Fig. 2c**). In addition, theta-gamma phase-amplitude coupling remained intact with depleted-TgCM infusion compared to WtCM infusion (from 1159.0 ± 277.6 to 1085.2 ± 258.6 MI, mean difference=-73.84, 95% CI [-228.31, 80.63], paired t(5)=-1.23, p=0.274, Cohen's d=-0.50. **Fig. 2d**).

In additional experiments, we infused 0.5 µL depleted-TgCM over 10 minutes, followed by 0.5 µL TgCM over 10 minutes as each animal ran on the linear track (**Fig.2e**). Animals ran significantly more laps during TgCM infusion than during depleted-TgCM infusion (from 12.3 ± 1.9 to 14.2 ± 2.2 laps, mean difference=1.83, 95% CI [0.03, 3.64], paired t(5)=2.61, p=0.048, Cohen's d=1.06. **Fig. 2f left**); running velocity was unchanged (from 5.5 ± 0.7 to 5.6 ± 0.6 cm/s, mean difference=0.12, 95% CI [-0.85, 1.10], paired t(5)=0.33, p=0.755, Cohen's d=0.13. **Fig. 2f right**). Compared to depleted-TgCM infusion, TgCM infusion reduced theta power but did not significantly affect gamma power (theta power: from 7.6 ± 1.8) × 10^{-3} to (6.5 ± 1.7) × 10^{-3}, mean difference=-1.08 × 10^{-3}, 95% CI [-1.89, -

0.27] × 10^{-3}, paired t(5)=-3.43, p=0.019, Cohen's d=-1.40; gamma power: from (7.5 ± 1.2) × 10^{-4} to (6.5 ± 0.9) × 10^{-4}, mean difference=-1.01 × 10^{-4}, 95% CI [-2.51, 0.49] × 10^{-4}, paired t(5)=-1.73, p=0.144, Cohen's d=-0.71. **Fig. 2g**). TgCM infusion decreased theta-gamma phase-amplitude coupling compared to depleted-TgCM (from 1113.6 ± 260.6 to 1020.0 ± 262.6 MI, mean difference=-93.59, 95% CI [-182.16, -5.02], paired t(5)=-2.72, p=0.042, Cohen's d=-1.11. **Fig. 2h**). Because animals ran slightly more laps during TgCM than during depleted-TgCM infusion (**Fig. 2f**), the accompanying reduction in theta-gamma coupling cannot be attributed to reduced locomotion.

These results show that AβOs, rather than other constituents of the Tg2576 culture medium, are the species responsible for disrupting theta-gamma coupling.

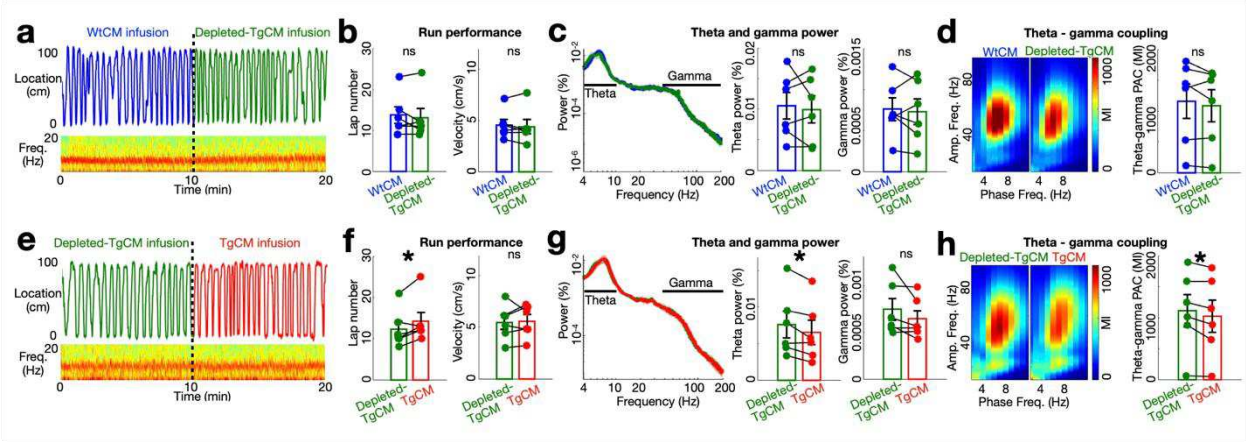


Figure 2. Aβ depletion abolished the AβO-induced theta-gamma coupling impairment. a) Examples of run behavior on the linear track as a function of time (top) and associated CA1 s. radiatum spectrograms (bottom) during WtCM infusion (blue), followed by depleted-TgCM infusion (green); representative data from one mouse. **b)** The number of laps run (left) and running velocity (right), **c)** theta and gamma band power,

and **d)** theta-gamma phase-amplitude coupling were comparable between WtCM and depleted-TgCM infusion. **e)** Examples of run behavior on the linear track as a function of time (top) and associated CA1 s. radiatum spectrograms (bottom) during depleted-TgCM infusion (green), followed by TgCM infusion (red); representative data from one mouse. **f)** The number of laps run (left) was increased with TgCM infusion compared to depleted-TgCM infusion; run velocity (right) was similar with TgCM and depleted-TgCM. **g)** Theta band power was decreased with TgCM infusion compared to depleted-TgCM infusion (left); gamma band power was comparable between depleted-TgCM and TgCM infusion. **h)** Theta-gamma phase-amplitude coupling was decreased with TgCM infusion compared to depleted-TgCM infusion. ns, $p>0.05$, * $p<0.05$, two-sided paired t-tests. n = 6 mice. Data are shown as mean ± SEM.

AβOs reduced activity in post-learning quiet wakefulness

During active exploration, AβOs impaired theta-gamma coupling without altering calcium event rates. Because quiet wakefulness supports learning and replay, we next asked whether AβOs also disrupt calcium activity during this offline state.

For this purpose, animals first ran on the linear track without infusion and then returned to their home cage, where they received a 10-minute infusion of 0.5 µL WtCM followed by a 10-minute infusion of 0.5 µL TgCM, while resting quietly (**Fig. 3a**). Delta power, ripple power, sharp wave ripple (SWR) rate and duration were comparable between WtCM infusion and TgCM infusion (delta power: from $(1.2 \pm 0.2) \times 10^{-2}$ to $(1.0 \pm 0.1) \times 10^{-2}$, mean difference=$-0.14 \times 10^{-2}$, 95% CI $[-0.64, 0.36] \times 10^{-2}$, paired $t(6)=-0.69$, $p=0.517$, Cohen's

d=-0.26; ripple power: from (5.3 ± 0.8) × 10^{-5} to (6.1 ± 1.6) × 10^{-5} , mean difference=0.87 × 10^{-5}, 95% CI [-1.99, 3.73] × 10^{-5}, paired t(6)=0.75, p=0.484, Cohen's d=0.28; SWR rate: from 0.1 ± 0.0 to 0.1 ± 0.0 event/s, mean difference=0.01, 95% CI [-0.01, 0.03], paired t(6)=1.67, p=0.146, Cohen's d=0.63; SWR length: from 0.2 ± 0.0 to 0.2 ± 0.0 s, mean difference=-0.00, 95% CI [-0.04, 0.04], paired t(6)=-0.20, p=0.848, Cohen's d=-0.08. **Fig. 3b**). Average calcium event rates of all cells, as well as place cells, were significantly reduced with TgCM infusion compared to WtCM infusion (all cells: from 3.0 ± 0.3 to 2.1 ± 0.2 spikes/min, mean difference=-0.91, 95% CI [-1.45, -0.36], paired t(4)=-4.62, p=0.010, Cohen's d=-2.06; place cells: from 3.2 ± 0.4 to 2.2 ± 0.3 spikes/min, mean difference=-0.98, 95% CI [-1.59, -0.38], paired t(4)=-4.51, p=0.011, Cohen's d=-2.02. **Fig. 3c**). Place cell pairwise reactivation was also reduced in the raw comparison between WtCM and TgCM infusion (from 0.2 ± 0.0 to 0.1 ± 0.0, mean difference=-0.09, 95% CI [-0.16, -0.01], paired t(4)=-3.15, p=0.035, Cohen's d=-1.41. **Fig. 3d**). To investigate whether this reflected reduced calcium activity rather than a specific effect on reactivation, we generated 500 surrogate WtCM datasets by randomly removing detected calcium events until each cell's event rate matched that observed during TgCM infusion. After rate matching, place cell reactivation during TgCM infusion did not differ significantly from that of the surrogate WtCM datasets (p=0.076, Monte Carlo, **Fig. 3e**), indicating no detectable effect of AβOs on reactivation beyond that expected from reduced activity.

To confirm the stability of calcium event rates and place cell reactivation, we repeated this experiment using sequential infusions of 0.5 µL aCSF as mice rested quietly after running on the track (**Fig. 3f**). Average calcium event rates of all cells, as well as place cells, were

comparable (all cells: from 1.9 ± 0.3 to 2.6 ± 0.3 spikes/min, mean difference=0.67, 95% CI [-0.16, 1.49], paired t(5)=2.08, p=0.092, Cohen's d=0.85; place cells: from 2.3 ± 0.6 to 2.7 ± 0.4 spikes/min, mean difference=0.44, 95% CI [-0.96, 1.84], paired t(4)=0.87, p=0.432, Cohen's d=0.39. **Fig. 3g**), and place cell reactivation remained intact (from 0.2 ± 0.0 to 0.2 ± 0.0, mean difference=0.04, 95% CI [-0.04, 0.12], paired t(4)=1.30, p=0.263, Cohen's d=0.58. **Fig. 3h**). Notably, all cell calcium rates during sequential aCSF infusions trended upward rather than downward (mean difference +0.67 spikes/min), opposite in sign to the reduction observed with TgCM (−0.91 spikes/min), indicating that nonspecific temporal drift cannot account for the AβO-associated hypoactivity.

These results show that AβOs reduce calcium activity during post-learning quiet wakefulness.

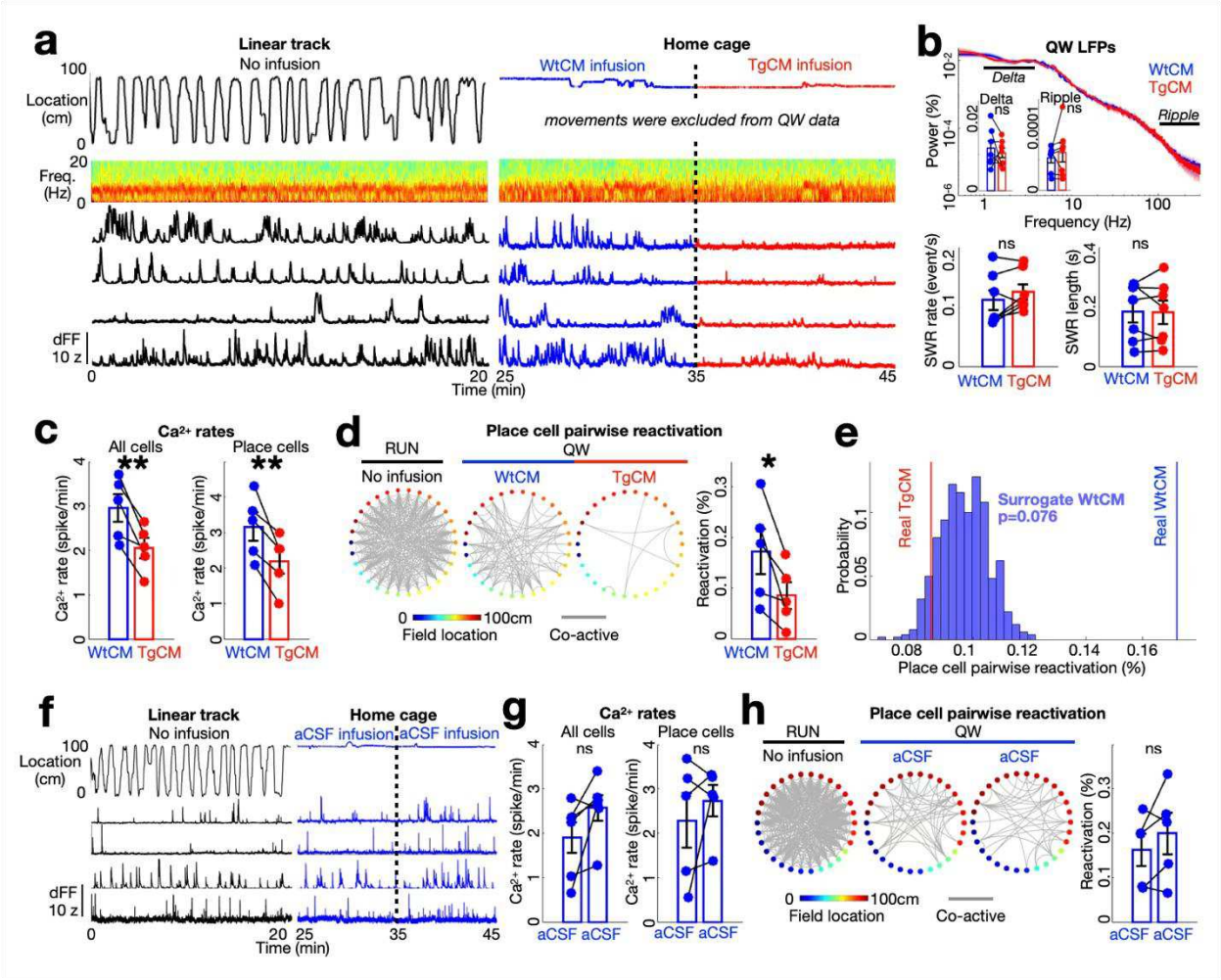


Figure 3. AβOs reduced calcium activity in post-learning quiet wakefulness. a) Animals ran on the linear track without infusion, returned to their home cage and then received sequential infusions of WtCM (blue) and TgCM (red). From top to bottom: Example of behavior on the linear track and subsequently in the home cage as a function of time, associated CA1 s. radiatum spectrograms and dynamic calcium traces; representative data from one mouse. **b)** In post-learning quiet wakefulness, delta band power, ripple band power, and sharp wave ripple rate and length were comparable between WtCM and TgCM infusion. **c)** In post-learning quiet wakefulness, average calcium event rates of all cells (left) and place cells (right) were reduced with infusion of

TgCM compared to WtCM. **d)** Place cell pairwise reactivation was reduced with TgCM infusion compared to WtCM infusion. In the example figures, each circle reflects a place cell with its color reflecting the location of the place field on the linear track. Lines connecting place cells indicate pairs with significant pairwise co-activity (see Methods). **e)** After randomly removing calcium events from cells during the WtCM infusion to match the calcium rates of TgCM infusion, 500 times (Surrogate WtCM), place cell reactivation with TgCM infusion was not significantly different from surrogate WtCM ($p = 0.076$, Monte Carlo, n = 500 surrogate datasets). **f)** Example of behavior and calcium traces when animals ran on the linear track without infusion, returned to their home cage and then received sequential infusions of aCSF (blue); representative data from one mouse. **g)** Calcium event rates for all cells and place cells were similar across sequential infusions of aCSF. **h)** Place cell reactivation remained unchanged across sequential aCSF infusions. ns, $p>0.05$, * $p<0.05$, ** $p<0.01$, two-sided paired t-tests except for the Monte Carlo analysis in (e). n = 7 mice for b; n = 5 mice, 348 ± 219 cells, and 50 ± 33 place cells for c, d, e; n = 6 mice, 253 ± 114 cells for g (left); n = 5 mice and 57 ± 26 place cells for g (right) and h. Data are shown as mean ± SEM.

Aβ depletion abolished AβO-induced reduction in calcium activity

To confirm the causal role of AβOs in these offline observations, we first compared infusion of 0.5 µL WtCM to infusion of 0.5 µL depleted-TgCM in quiet wakefulness following run behavior (**Fig. 4a)**. Average calcium event rates of all cells, as well as place cells, were similar across these manipulations (depleted-TgCM infusion vs WtCM infusion: all cells: from 2.4 ± 0.7 to 1.9 ± 0.6 spikes/min, mean difference=-0.48, 95% CI [-2.06,

1.11], paired t(5)=-0.77, p=0.475, Cohen's d=-0.32; place cells: from 2.5 ± 0.6 to 1.8 ± 0.8 spikes/min, mean difference=-0.76, 95% CI [-2.83, 1.31], paired t(4)=-1.02, p=0.366, Cohen's d=-0.46. **Fig. 4b**). Place cell pairwise reactivation also remained comparable (depleted-TgCM vs WtCM infusion: from 0.1 ± 0.1 to 0.0 ± 0.0, mean difference=-0.08, 95% CI [-0.27, 0.12], paired t(3)=-1.25, p=0.299, Cohen's d=-0.63. **Fig. 4c**).

Next, we sequentially infused 0.5 µL depleted-TgCM and 0.5 µL TgCM in post-learning quiet wakefulness (**Fig. 4d**). TgCM infusion reduced place cell calcium event rates compared to depleted-TgCM infusion (from 2.6 ± 0.3 to 1.8 ± 0.3 spikes/min, mean difference=-0.78, 95% CI [-1.25, -0.31], paired t(3)=-5.33, p=0.013, Cohen's d=-2.67), with a concordant but nonsignificant reduction across all cells (from 3.8 ± 0.9 to 2.2 ± 0.5 spikes/min , mean difference=-1.57, 95% CI [-3.22, 0.09], paired t(5)=-2.44, p=0.059, Cohen's d=-0.99; **Fig. 4e**). We did not detect an effect of TgCM on place cell reactivation compared to depleted-TgCM (from (10.0 ± 5.2) × 10^{-2} to (6.6 ± 2.6) × 10^{-2}, mean difference=-3.40 × 10^{-2}, 95% CI [-13.06, 6.27] × 10^{-2}, paired t(3)=-1.12, p=0.345, Cohen's d=-0.56. **Fig. 4f**).

Together with the WtCM-TgCM comparison, these results support a specific effect of AβOs on calcium activity in quiet wakefulness.

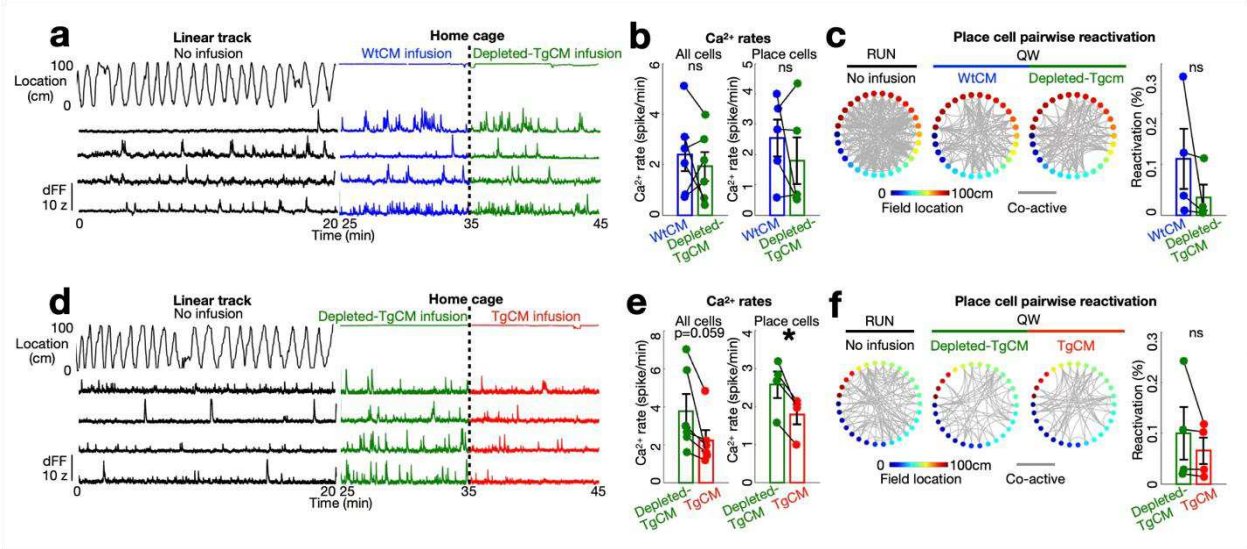


Figure 4. Aβ depletion abolished AβO-induced hypoactivity. a) Example of behavior and calcium traces when animals ran on the linear track without infusion, returned to their home cage and then received sequential infusion of WtCM (blue) and depleted-TgCM (green); representative data from one mouse. **b)** In quiet wakefulness after running on the track, calcium rates of all cells and place cells were unaffected by infusion of depleted-TgCM infusion compared to WtCM infusion. **c)** Infusion of depleted-TgCM did not significantly affect place cell pairwise reactivation compared to WtCM. **d)** Example of behavior and calcium traces when animals ran on the linear track without infusion, returned to their home cage and then received sequential infusion of depleted-TgCM (green) and TgCM (red); representative data from one mouse. **e)** All cell calcium rates showed a concordant but nonsignificant reduction with TgCM infusion compared with depleted-TgCM infusion. Place cell calcium rates were significantly reduced. The place cell comparison includes fewer mice because sessions with fewer than 10 detected place cells were excluded from place cell analyses (see Methods). **f)** Place cell pairwise reactivation was unaffected by infusion of TgCM compared to depleted-TgCM. ns, $p>0.05$, * $p<0.05$, two-sided paired t-tests. n = 6 mice and 298 ± 166 cells for b (left); n = 5 mice

and 92 ± 52 place cells for b (right); n = 4 mice and 117 ± 61 place cells for c; n = 6 mice and 554 cells for e (left); n = 4 mice and 186 ± 102 place cells for e (right) and f. Data are shown as mean ± SEM.

AβOs at physiological concentrations did not cause hyperactivity under anesthesia

Prior studies have reported AβO-induced hyperactivity under anesthesia using synthetic Aβ [36]. Using the same synthetic AβO preparation and concentration (100 nM) under matching 1% isoflurane anesthesia, synthetic AβOs significantly increased calcium event rates compared to aCSF (from 3.1 ± 1.1 to 4.5 ± 1.0 spikes/min, mean difference=1.37, 95% CI [0.23, 2.50], paired t(3)=3.82, p=0.032, Cohen's d=1.91. **Fig. 5a**). In contrast, TgCM infusion did not significantly alter calcium event rates compared to WtCM at physiologically relevant AβO concentrations (3.64 nM, from the same TgCM batch used throughout this study; from 4.5 ± 0.6 to 4.3 ± 0.5 spikes/min, mean difference=-0.20, 95% CI [-1.63, 1.23], paired t(5)=-0.36, p=0.736, Cohen's d=-0.15. **Fig. 5b**).

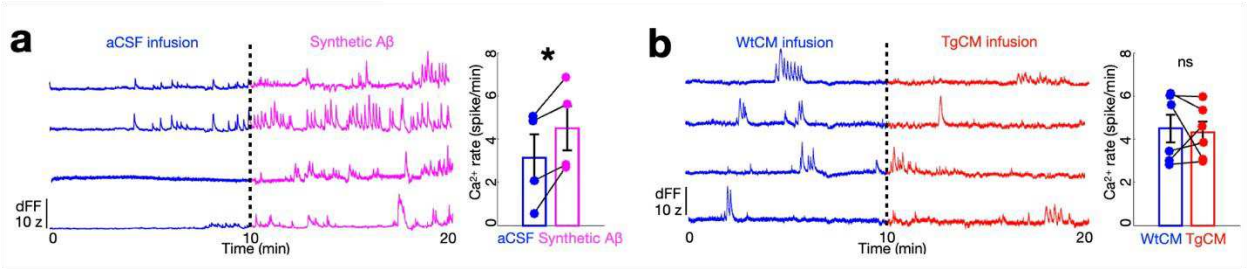


Figure 5. AβOs at physiological concentrations did not cause hyperactivity under anesthesia. a) Left: example of calcium traces under 1% isoflurane as animals received sequential infusions of aCSF (blue) and synthetic Aβ (magenta). Right: synthetic AβOs increased calcium event rates compared to aCSF. **b)** Left: example of calcium traces under 1% isoflurane as animals received sequential infusion of WtCM (blue) and TgCM

(red). Right: Calcium event rates were comparable between WtCM and TgCM infusion. ns, $p>0.05$, * $p<0.05$, two-sided paired t-tests. n = 4 mice and 143 ± 89 cells for a; n = 6 mice and 350 ± 144 cells for b. Data are shown as mean ± SEM.

Discussion

Aβ plaques are the defining pathological hallmark of AD [1,2], yet plaque levels correlate poorly with dementia severity, and anti-amyloid antibody therapies that clear plaques produce only modest slowing of cognitive decline [4–7]. This gap suggests that plaque-independent mechanisms, such as tau pathology, disrupted Aβ metabolism, and soluble Aβ species, contribute meaningfully to disease progression. We tested the hypothesis that soluble AβOs, a toxic misfolded Aβ species upstream of amyloid plaques, disrupt hippocampal circuit function independently of amyloid plaques.

AβOs are synaptotoxic at the cellular level, disrupting NMDA receptor signaling, remodeling synapses, degrading dendritic spines, and impairing plasticity [9–18]. Whether and how these cellular effects scale to systems-level circuit dysfunction has not been established. By combining live intrahippocampal infusions with simultaneous calcium imaging and electrophysiology in freely behaving mice, this study directly observed hippocampal circuit responses to AβOs as they occurred, without anesthesia or restraint, across both an encoding-relevant active behavioral state and a consolidation-relevant offline state. We focused on established hippocampal circuit signatures of memory, theta-gamma phase-amplitude coupling during encoding [19–22] and place cell reactivation during offline consolidation and planning [23–25], together with neuronal activity, which together

constituted our three prespecified primary outcomes. Because reactivation depends on ongoing neuronal activity, we designed our offline experiments to distinguish a specific effect of AβOs on reactivation from a secondary consequence of reduced activity.

We found that AβO effects on hippocampal circuit function depended on behavioral state. During active exploration, AβOs reduced theta-gamma coupling without altering running behavior, calcium event rates, or place cell properties, indicating a preferential effect on oscillatory coupling rather than a general disruption of hippocampal function. Theta power was also modestly reduced in the depletion-repletion comparison. Because the modulation index is computed from the phase of the theta-band signal rather than its amplitude, reduced theta power is unlikely to account for the coupling deficit, and gamma power was unchanged throughout. Aβ depletion preserved theta-gamma coupling, whereas subsequent TgCM infusion again impaired it. During post-learning quiet wakefulness, TgCM reduced calcium event rates relative to WtCM. This effect was absent after Aβ depletion and reappeared with TgCM re-exposure. Place cell reactivation was also lower in the raw WtCM-TgCM comparison, but this difference did not survive resampling to match calcium rates and was not reproduced in the depletion-repletion comparison. Because only four animals contributed to the depletion-repletion reactivation analysis, this comparison had limited sensitivity to detect a small activity-independent effect of AβOs on place cell reactivation. The rate-matched Monte Carlo analysis therefore provides the most informative basis for concluding that we did not detect an effect of AβOs on reactivation beyond that expected from reduced activity. The observation of TgCM-induced hypoactivity in quiet wakefulness is consistent with our

observation of reduced calcium activity in young APP/PS1 mice before significant plaque deposition [37]. AβO-induced hypoactivity is therefore an offline phenotype supported by the convergent WtCM-TgCM and depletion experiments, and a tractable therapeutic target. Beyond these circuit measures, we also examined hyperactivity, a separately reported hippocampal phenotype in AD models that is usually observed under anesthesia using synthetic AβOs [36]. Using the same synthetic AβO preparation and concentration under matching anesthesia, we reproduced this hyperactivity relative to aCSF, but TgCM produced no such effect relative to WtCM at physiological concentrations. These observations suggest that hyperactivity attributed to AβOs in prior work may reflect the high concentrations used in synthetic preparations rather than an effect of naturally occurring AβOs at disease-relevant levels. Because these experiments differed in both preparation and concentration, however, their relative contributions cannot be disentangled here. A dose-matched comparison of synthetic and naturally occurring AβOs would be required.

Three methodological choices distinguish this study from prior work on AβOs. First, we used TgCM, which contains naturally occurring, low molecular weight human AβOs, rather than synthetic or recombinant Aβ preparations that may differ structurally from naturally occurring AβOs and are typically applied at concentrations well above those found in brain. TgCM has previously been shown to reproduce synaptic phenotypes attributable to AβOs [9,38]. Second, we infused AβO-containing medium directly into nontransgenic hippocampus rather than employing a transgenic amyloidosis model. Although we previously observed circuit disruption in young APP/PS1 mice when AβOs

are elevated but plaques are minimal [37], APP overexpression and the PS1 mutation carry non-amyloid consequences that could independently affect neuronal function [26–34]. Pairing TgCM with vehicle (WtCM) and immunodepleted (depleted-TgCM) conditions within the same animal also isolates the contribution of Aβ from other constituents of the culture media and from genetic background. Combined with simultaneous calcium imaging and electrophysiology during live infusion and free behavior, these design choices allowed us to evaluate the contribution of Aβ to hippocampal circuit dysfunction directly across online-offline states.

This study has several limitations. We did not include a behavioral memory test, because the infusion system's slow flow rate and narrow tubing precluded the use of larger arenas that standard memory tasks require. As a result, the circuit phenotypes reported here, which are established correlates of memory encoding and consolidation, are not linked to explicit tests of memory function in the same animals. We also did not acquire sleep data, given concern that the extended latency to sleep onset in our home-cage setup would allow the AβOs to degrade in the infusion reservoir at room temperature. Our post-learning quiet wakefulness recordings are therefore a partial proxy for offline consolidation. Additionally, because our recordings were restricted to the infusion period itself, we were unable to evaluate persistent or chronic circuit consequences of AβO exposure.

Due to the complexity of the preparation, sample sizes are modest, and some effects were of borderline significance. We prespecified three primary hypotheses based on our

prior work in APP/PS1 mice [37]: that AβOs would impair PAC during exploration, and that AβOs would reduce calcium activity and place cell reactivation offline. The PAC and activity hypotheses were supported; the reactivation hypothesis was not supported once calcium rate was accounted for. Prespecification reduces but does not eliminate the risk of false-positive findings across the full set of contrasts. We used only male mice of a single strain and a single source of AβOs. Whether these findings extend to females, other genetic backgrounds, or other AβO species or conformations remains to be tested.

In summary, naturally occurring AβOs infused into nontransgenic hippocampus at disease-relevant concentrations impaired theta-gamma coupling during active exploration and reduced neuronal activity during post-learning quiet wakefulness. Both of these effects were reversed by Aβ depletion. As these circuit disruptions occurred independent of plaque formation, AβO-targeted interventions could preserve or restore hippocampal circuit function at a disease stage that precedes substantial plaque burden, earlier than current plaque-clearing therapies may allow. AβO-selective antibodies such as sabirnetug (ACU193) are now in phase 2 clinical trials [39], and these findings provide additional mechanistic rationale for this approach.

Methods

All procedures were approved by the Institutional Animal Care and Use Committees of the Massachusetts General Hospital. The study was conducted in accordance with the ethical guidelines of the US National Institutes of Health.

Culture media: Wild type culture medium (WtCM), transgenic culture medium (TgCM), and TgCM with Aβ depletion (depleted-TgCM) were prepared as previously described [9]: TgCM and WtCM were prepared from primary cortical neuronal cultures derived from Tg2576 or wild type mouse embryos. The pregnant female was euthanized at E14.5, and embryos were collected. Embryonic cortices were isolated and dissociated using the Papain Dissociation System (Worthington Biochemical Corp.), according to the manufacturer's protocol. Tissue from each embryo was collected and submitted to Transnetyx, Inc. (Cordova, TN, USA) for genotyping. Dissociated cortical cells were seeded on poly-D-lysine (PDL)-coated culture plates (EMD Millipore Corp Inc.), 1:50, in Neurobasal medium (Invitrogen), supplemented with 2% B27 (Invitrogen), 2 mM GlutaMAX (Gibco), 100 U/mL penicillin (Gibco), 100 µg/mL streptomycin (Gibco), and 10% FBS (Gibco). Cultures were maintained at 37°C with 5% CO_2. The following day, the medium was replaced with FBS-free Neurobasal-based growth medium and cultures were maintained until 14 days in vitro (DIV). Culture media was collected at 14 DIV and centrifuged at 2500 rpm for 10 min at 4°C, aliquoted, and stored at −80°C. To immunodeplete Aβ from TgCM, protein G sepharose beads (Cytiva cat#28-9513-79) were initially rinsed with chilled Neurobasal medium and mixed with 1 ml of TgCM for 30 min at 4°C under agitation to prevent non-specific interactions. Following centrifugation, the beads were removed. The supernatant was then combined with 9 µg of 6E10 antibody (Biolegend cat# SIG-39320) and 100 µl pre-washed protein G beads and incubated overnight at 4°C with continuous shaking. The Aβ content was confirmed by molecular weight cut-off filter, size exclusion chromatography (SEC), and human Aβ ELISA (Wako #298-64601), following the manufacturer's instructions. SEC showed that low-weight

AβOs (<75kDa) are the primary species in TgCM. The final Aβ concentration was 0.08 nM in WtCM, 3.64 nM in TgCM, and 0.12 nM in depleted-TgCM. All WtCM, TgCM, and depleted-TgCM aliquots used in this study were from the same culture batch.

Synthetic Aβ preparation: Synthetic Aβ40S26C dimers (Anaspec Cat# AS-63671-1) were dissolved in DMSO and diluted to 100 nM in aCSF [36].

Lens-electrode-cannula device: Tungsten wires (0.002” diameter) were connected to an Electrode Interface Board with 8 channels (EIB-8, Neuralynx). The electrode wires, an integrated GRIN lens with miniscope baseplate (Inscopix), and a cannula (26G) were bonded together using metabond (C&B). To ensure that the infusion was close to the imaging window and LFP recording sites, the cannula tip was placed within ~1 mm of the lens, with the electrodes immediately below to sample the pyramidal cell layer and s. radiatum. A 30G tungsten wire was used as a stylus to prevent cannula clogging.

Surgery: The surgical procedure was similar to our previous publications [37,40,41]. Briefly, animals (3 month old male C57BL/6J mice, Jackson Laboratory, strain 000664) underwent injection of 1 μL AAV1-hSyn-GCaMP6f, targeting the hippocampal CA1 region (ML 1.5 mm, AP -2.1 mm, DV -1.5 mm). Two weeks later, the integrated lens-electrode-cannula device was implanted (ML 1.5 mm, AP -2.1 mm, DV -1.2 mm), with cerebellar ground. The implant was secured by metabond and skull screws. Recordings began two weeks after implantation, when mice were approximately 4 months old.

Infusion and recording: Fresh aliquots of WtCM, TgCM or depleted-TgCM were used for each experiment. The infusion system consisted of a 5 μL syringe mounted on a syringe pump, connected to PE-10 tubing and a 30-gauge needle. The infusion needle was engineered to extend 500μm from the cannula tip to prevent infusion backflow. The syringe, tubing, and infusion needle were first flushed and filled with sterile aCSF. A small volume of air was back drawn through the distal infusion needle tip into the system, followed by the culture media, to serve as a marker of movement. It stayed upstream of the culture media and was never infused into the brain. A total volume of 1 μL of culture media was infused at 0.05μL/min. Calcium imaging, electrophysiology and animal position were recorded simultaneously and continuously during the infusion as animals ran on a linear track or rested in the home cage. At the end of each experiment, a new stylus was inserted into the cannula to prevent clogging. Because incomplete washout of AβO effects during a subsequent aCSF or depleted-TgCM infusion could confound subsequent experiments, infusion order was not counterbalanced across experiments. We instead used sequential aCSF-aCSF infusions to test directly for nonspecific temporal drift over paired acquisitions.

Anesthetized recording: Mice were maintained under 1% isoflurane in oxygen delivered at 1.0 L/min flow rate through a nose cone. Body temperature was maintained at 37 ℃ with a controlled warming pad (Kent Scientific). Calcium imaging was acquired through the chronically implanted GRIN lens. aCSF - Synthetic AβOs (100 nM), and in separate experiments WtCM - TgCM, were infused sequentially through the implanted cannula at 0.05 μL/min for 20 min as described above. Imaging began immediately after infusion

started and ended immediately after infusion ended, and conditions were separated at midpoint of the infusion and recording (10 min). The aCSF - Synthetic AβO cohort and the WtCM – TgCM cohort were independent.

Data Analysis: All analyses were performed in MATLAB 2024b and were similar to those described in our previous publications [37,40,41].

Position videos (Neuralynx): Animal position was recorded from an overhead camera sampled at 30 Hz and was used to identify each animal's behavior: Run was defined as velocity > 1 cm/s on the linear track, and quiet wakefulness was defined as velocity < 0.5 cm/s in the home cage in the absence of sleep.

Electrophysiology recordings (Neuralynx): Raw LFPs were recorded at 32 kHz and down sampled to 1 kHz offline. The spectrograms of each channel were calculated using the Chronux toolbox [42] (moving window = 2 s, step size = 1 s). The channel with the strongest theta oscillations was assigned to s. radiatum and used to evaluate delta, theta and gamma oscillations. The channel with the greatest SWR incidence was assigned to s. pyramidale and used to quantify SWR rate and duration. Power spectra were computed from 0.5 to 200 Hz using the Chronux toolbox [42], and the sum of relative power of delta (1 – 4 Hz), theta (4 – 10 Hz), gamma (30 – 200 Hz) and ripple (100 – 300 Hz) were used for quantification. Phase-amplitude-coupling (PAC) modulation index (MI) was calculated with 1–25 Hz for phase frequency and 1–300 Hz for amplitude frequency [43,44], and the mean value of the high coupling region was used for quantification [45].

Calcium imaging (Inscopix): Calcium imaging was recorded at 20 Hz using the lowest LED power compatible with cell detection, in recording blocks of up to 20 minutes to limit

photobleaching. A TTL pulse was sent with each imaging frame and recorded by Neuralynx to enable offline temporal synchronization of calcium imaging, electrophysiology, and position datasets. Dynamic calcium imaging raw videos were spatially band passed and motion corrected by Inscopix Data Processing Software (IDPS). Cells were then identified by CNMFe [46], and calcium events were detected at 2 Z scores above the mean [37,40,41]. During running (>1 cm/s), cells were classified as place cells when their spatial information exceeded the 95th percentile of a null distribution generated from 1,000 shuffles in which each cell's calcium events were randomly reassigned to time points within the corresponding running epochs (Monte Carlo $p<0.05$) [37,47]. Place fields were defined at 50% of the peak event rate distribution across track location [48]. Place cell pairwise reactivation was defined as a pair with peak calcium event cross-correlation > 0.001, using 0.1 s bins and a ± 3 s lag window, during both online and offline behavior [37]. Recordings containing at least 10 place cells were included in the pairwise reactivation analysis. Sample sizes therefore differ across analyses within the same cohort: sessions in which fewer than 10 place cells were detected were excluded from place cell and reactivation analyses, and sessions without adequate cell detection across both infusion epochs were excluded from calcium rate analyses. The number of animals contributing to each comparison is given in the corresponding figure legend.

Statistical analyses: Based on prior observations in young APP/PS1 mice before substantial accumulation of amyloid plaques demonstrating reduced phase-amplitude coupling in awake behavior, and reduced calcium activity and place cell pairwise reactivation in offline behavior compared to littermate controls [37], we prespecified three

primary hypotheses: that AβOs would impair PAC during exploration and reduce calcium activity and place cell pairwise reactivation during quiet wakefulness. All other comparisons were considered secondary. No correction for multiple comparisons was applied to the three primary hypothesis tests, each assessed with a single confirmatory comparison. For secondary analyses, we report exact p values, confidence intervals, and effect sizes for all comparisons. Sample sizes were informed by prior studies using comparable experimental approaches and outcomes. All comparisons were performed within subjects, with each animal serving as its own control. All paired comparisons were evaluated using two-sided tests, including the prespecified directional hypotheses, as a conservative approach. For each test, we report the mean difference, 95% confidence interval, t statistic with degrees of freedom, exact p value, and effect size (Cohen's d). For the rate-matched reactivation analysis, the Monte Carlo p value was defined as the proportion of the 500 surrogate WtCM datasets in which place cell pairwise reactivation was less than or equal to the observed TgCM value. Secondary comparisons were not corrected for multiple comparisons and are considered exploratory. The within-subject sequential infusion design precluded blinding to infusion order; calcium event detection and place cell classification used automated pipelines with fixed, prespecified thresholds applied identically across conditions. Statistical significance was defined as $p < 0.05$. Data are presented as mean ± SEM.

Data and Code Availability

The source data and analysis code supporting this study are available at https://doi.org/10.7910/DVN/0TNVIG.

Author Contributions

Conceptualization, HL and SNG; Methodology, HL, AF, SSH and SNG; Software, HL and SNG; Validation, HL; Formal Analysis, HL; Investigation, HL; Resources, HL, AF, SA, ZV, MY, KVK and SNG. Data Curation, HL; Writing – Original Draft, HL; Writing – Review & Editing, HL, AF, SA, ZV, SSH, MY, KVK and SNG; Visualization, HL; Supervision, SNG; Project Administration, HL and SNG; Funding Acquisition, HL and SNG.

Sources of Funding

This work was supported by Alzheimer's Association grant to HL (AARF-25-1484358) and NIH grants to KVK (RF1 AG098887) and SNG (R01 AG077611).

Competing Interests

The authors declare no competing interests.

References

1. Bloom, G. S. Amyloid-β and Tau: The Trigger and Bullet in Alzheimer Disease Pathogenesis. *JAMA Neurol.* **71**, 505–508 (2014).
2. Murphy, M. P. & LeVine, H. Alzheimer's Disease and the β-Amyloid Peptide. *J. Alzheimers Dis. JAD* **19**, 311 (2010).
3. Terry, R. D. *et al.* Physical basis of cognitive alterations in Alzheimer's disease: synapse loss is the major correlate of cognitive impairment. *Ann. Neurol.* **30**, 572–580 (1991).

4. Mintun, M. A. *et al.* Donanemab in Early Alzheimer's Disease. *N. Engl. J. Med.* **384**, 1691–1704 (2021).
5. Budd Haeberlein, S. *et al.* Two Randomized Phase 3 Studies of Aducanumab in Early Alzheimer's Disease. *J. Prev. Alzheimers Dis.* **9**, 197–210 (2022).
6. van Dyck, C. H. *et al.* Lecanemab in Early Alzheimer's Disease. *N. Engl. J. Med.* **388**, 9–21 (2023).
7. Sims, J. R. *et al.* Donanemab in Early Symptomatic Alzheimer Disease: The TRAILBLAZER-ALZ 2 Randomized Clinical Trial. *JAMA* **330**, 512–527 (2023).
8. McLean, C. A. *et al.* Soluble pool of Aβ amyloid as a determinant of severity of neurodegeneration in Alzheimer's disease. *Ann. Neurol.* **46**, 860–866 (1999).
9. Arbel-Ornath, M. *et al.* Soluble oligomeric amyloid-β induces calcium dyshomeostasis that precedes synapse loss in the living mouse brain. *Mol. Neurodegener.* **12**, 27 (2017).
10. Cleary, J. P. *et al.* Natural oligomers of the amyloid-β protein specifically disrupt cognitive function. *Nat. Neurosci.* **8**, 79–84 (2005).
11. Cline, E. N., Bicca, M. A., Viola, K. L. & Klein, W. L. The Amyloid-β Oligomer Hypothesis: Beginning of the Third Decade. *J. Alzheimers Dis.* **64**, S567–S610 (2018).
12. Ding, Y. *et al.* Amyloid Beta Oligomers Target to Extracellular and Intracellular Neuronal Synaptic Proteins in Alzheimer's Disease. *Front. Neurol.* **10**, (2019).
13. Faucher, P., Mons, N., Micheau, J., Louis, C. & Beracochea, D. J. Hippocampal Injections of Oligomeric Amyloid β-peptide (1–42) Induce Selective Working

Memory Deficits and Long-lasting Alterations of ERK Signaling Pathway. *Front. Aging Neurosci.* **7**, (2016).

14. Ferreira, S. T., Lourenco, M. V., Oliveira, M. M. & De Felice, F. G. Soluble amyloid-β oligomers as synaptotoxins leading to cognitive impairment in Alzheimer's disease. *Front. Cell. Neurosci.* **9**, 191 (2015).
15. Nicole, O. *et al.* Soluble amyloid beta oligomers block the learning-induced increase in hippocampal sharp wave-ripple rate and impair spatial memory formation. *Sci. Rep.* **6**, 22728 (2016).
16. Özcan, G. G., Lim, S., Leighton, P. L., Allison, W. T. & Rihel, J. Sleep is bi-directionally modified by amyloid beta oligomers. *eLife* **9**, e53995 (2020).
17. Shankar, G. M. *et al.* Amyloid-β protein dimers isolated directly from Alzheimer's brains impair synaptic plasticity and memory. *Nat. Med.* **14**, 837–842 (2008).
18. Malinow, R. & Malenka, R. C. AMPA receptor trafficking and synaptic plasticity. *Annu. Rev. Neurosci.* **25**, 103–126 (2002).
19. Belluscio, M. A., Mizuseki, K., Schmidt, R., Kempter, R. & Buzsaki, G. Cross-Frequency Phase-Phase Coupling between Theta and Gamma Oscillations in the Hippocampus. *J. Neurosci.* **32**, 423–435 (2012).
20. Buzsáki, G. Theta Oscillations in the Hippocampus. *Neuron* **33**, 325–340 (2002).
21. Buzsáki, G. Theta rhythm of navigation: Link between path integration and landmark navigation, episodic and semantic memory. *Hippocampus* **15**, 827–840 (2005).
22. Colgin, L. L. Rhythms of the hippocampal network. *Nat. Rev. Neurosci.* **17**, 239–249 (2016).

23. Ólafsdóttir, H. F., Bush, D. & Barry, C. The Role of Hippocampal Replay in Memory and Planning. *Curr. Biol.* **28**, R37–R50 (2018).
24. Harvey, R. E., Robinson, H. L., Liu, C., Oliva, A. & Fernandez-Ruiz, A. Hippocampo-cortical circuits for selective memory encoding, routing, and replay. *Neuron* **111**, 2076-2090.e9 (2023).
25. Davidson, T. J., Kloosterman, F. & Wilson, M. A. Hippocampal Replay of Extended Experience. *Neuron* **63**, 497–507 (2009).
26. Shen, J. & Kelleher, R. J. The presenilin hypothesis of Alzheimer's disease: Evidence for a loss-of-function pathogenic mechanism. *Proc. Natl. Acad. Sci.* **104**, 403–409 (2007).
27. Thinakaran, G. The role of presenilins in Alzheimer's disease. *J. Clin. Invest.* **104**, 1321–1327 (1999).
28. Ho, A. & Shen, J. Presenilins in synaptic function and disease. *Trends Mol. Med.* **17**, 617–624 (2011).
29. Zhang, D. *et al.* Inactivation of presenilins causes pre-synaptic impairment prior to post-synaptic dysfunction. *J. Neurochem.* **115**, 1215–1221 (2010).
30. Zhang, C. *et al.* Presenilins are essential for regulating neurotransmitter release. *Nature* **460**, 632–636 (2009).
31. Saura, C. A. *et al.* Loss of presenilin function causes impairments of memory and synaptic plasticity followed by age-dependent neurodegeneration. *Neuron* **42**, 23–36 (2004).

32. Wu, B., Yamaguchi, H., Lai, F. A. & Shen, J. Presenilins regulate calcium homeostasis and presynaptic function via ryanodine receptors in hippocampal neurons. *Proc. Natl. Acad. Sci.* **110**, 15091–15096 (2013).
33. Jankowsky, J. L. *et al.* Mutant presenilins specifically elevate the levels of the 42 residue β-amyloid peptide in vivo: evidence for augmentation of a 42-specific γ secretase. *Hum. Mol. Genet.* **13**, 159–170 (2004).
34. Jankowsky, J. L. *et al.* Co-expression of multiple transgenes in mouse CNS: a comparison of strategies. *Biomol. Eng.* **17**, 157–165 (2001).
35. Li, H. & McConnell, G. C. Intraoperative Microelectrode Recordings in Substantia Nigra Pars Reticulata in Anesthetized Rats. *Front. Neurosci.* **14**, (2020).
36. Busche, M. A. *et al.* Critical role of soluble amyloid-β for early hippocampal hyperactivity in a mouse model of Alzheimer's disease. *Proc. Natl. Acad. Sci.* **109**, 8740–8745 (2012).
37. Li, H. *et al.* Impaired hippocampal circuit function underlying memory encoding and consolidation precede robust Aβ deposition in a mouse model of alzheimer's disease. *Sci. Rep.* **15**, 21957 (2025).
38. Hudry, E. *et al.* Inhibition of the NFAT Pathway Alleviates Amyloid Beta Neurotoxicity in a Mouse Model of Alzheimer's Disease. *J. Neurosci.* **32**, 3176–3192 (2012).
39. Siemers, E. *et al.* INTERCEPT-AD, a phase 1 study of intravenous sabirnetug in participants with mild cognitive impairment or mild dementia due to Alzheimer's disease. *J. Prev. Alzheimers Dis.* **12**, 100005 (2025).

40. Zhou, H. *et al.* Cholinergic modulation of hippocampal calcium activity across the sleep-wake cycle. *eLife* **8**, e39777 (2019).
41. Zhou, H. *et al.* Disruption of hippocampal neuronal circuit function depends upon behavioral state in the APP/PS1 mouse model of Alzheimer's disease. *Sci. Rep.* **12**, 21022 (2022).
42. Bokil, H., Andrews, P., Kulkarni, J. E., Mehta, S. & Mitra, P. P. Chronux: A platform for analyzing neural signals. *J. Neurosci. Methods* **192**, 146–151 (2010).
43. Onslow, A. C. E., Bogacz, R. & Jones, M. W. Quantifying phase–amplitude coupling in neuronal network oscillations. *Prog. Biophys. Mol. Biol.* **105**, 49–57 (2011).
44. Osipova, D., Hermes, D. & Jensen, O. Gamma Power Is Phase-Locked to Posterior Alpha Activity. *PLoS ONE* **3**, e3990 (2008).
45. Zhurakovskaya, E. *et al.* Impaired hippocampal-cortical coupling but preserved local synchrony during sleep in APP/PS1 mice modeling Alzheimer's disease. *Sci. Rep.* **9**, 5380 (2019).
46. Zhou, P. *et al.* Efficient and accurate extraction of in vivo calcium signals from microendoscopic video data. *eLife* **7**, e28728 (2018).
47. Markus, E. J., Barnes, C. A., McNaughton, B. L., Gladden, V. L. & Skaggs, W. E. Spatial information content and reliability of hippocampal CA1 neurons: Effects of visual input. *Hippocampus* **4**, 410–421 (1994).
48. Go, M. A. *et al.* Place Cells in Head-Fixed Mice Navigating a Floating Real-World Environment. *Front. Cell. Neurosci.* **15**, (2021).

Supplementary Files

This is a list of supplementary files associated with this preprint. Click to download.

- Supplementaryncfinal.docx